Supplement of Atmos. Chem. Phys., 23, 7699–7717, 2023
https://doi.org/10.5194/acp-23-7699-2023-supplement

Atmospheric Chemistry and Physics
Open Access
EGU

Supplement of

Trajectory enhancement of low-earth orbiter thermodynamic retrievals to predict convection: a simulation experiment

Mark T. Richardson et al.

Correspondence to: Mark T. Richardson (markr@jpl.nasa.gov)

1 CAPE across products and sensitivity to resolution

The standard CAPE definition is:

$$CAPE = g\int_{LFC}^{LNB}\frac{T_v - T_{v,env}}{T_{v,env}}dz \quad (1)$$

Where the g is acceleration due to gravity, LFC the level of free convection, LNB the level of neutral buoyancy, T_v the virtual temperature and the subscript *env* means the environmental profile. The main paper uses the *most unstable* (MU) parcel, defined as the parcel with the largest CAPE. Computationally, the integral is approximated via summation and the result may depend on the vertical resolution of the calculation. The vertical resolution can also change the selected parcel and derived LFC and LNB, as may horizontal averaging of profiles prior to the calculation.

The products considered in this study have different spatial resolutions.

i. ERA5 CAPE is calculated from the 137 model levels at 31 km horizontal resolution.

ii. ERA5 3-D fields from the Copernicus data store have 27 levels from 100 hPa—surface, with ΔP from 25—50 hPa. Horizontal resolution is 0.25° latitude-longitude.

iii. The AIRS L2Sup ΔP is 7—28 hPa between 100—1,100 hPa. Horizontal resolution is 13.5 km at nadir and almost 40 km at the swath edge.

iv. AIRS-FCST reports at ΔP =30 hPa and 1° latitude-longitude horizontal resolution.

The ERA5 product CAPE is calculated at the finest vertical resolution across all products, but for computational efficiency it uses a different calculation method:

$$CAPE \approx g\int_{z_{dep}}^{z_{top}}\frac{\theta_{ep} - \overline{\theta}_{env,sat}}{\overline{\theta}_{env,sat}}dz \quad (2)$$

In this case the parcel's equivalent potential temperature θ_{esat} is used in place of its T_v and the environmental saturated equivalent potential temperature $\overline{\theta}_{esat}$ in place of $T_{v,env}$. CAPE is then calculated from each model level up to z_{top}, which is defined at the 350 hPa surface. The parcel with the highest CAPE, i.e. the MU parcel is kept. However, due to the differences between Eqs. (1) and (2), it is possible that the selected parcel could differ, or even for the same parcel the calculated CAPE might not be the same.

We make the following comparisons to identify changes in calculated CAPE:

1. ERA5 product versus SHARPpy calculated MU_CAPE using the ERA5 3-D fields at 0.25° latitude-longitude resolution. The main difference here will be from algorithm differences and *vertical* resolution,
2. ERA5 product versus SHARPpy MU_CAPE using ERA5 3-D fields at 1° latitude-longitude resolution. Any differences beyond those shown in step 1 above will be due to changes in *horizontal* resolution
3. ERA5 product versus SHARPpy MU_CAPE calculated from the 3-D ERA5-overpass fields. Any further differences beyond those seen in step 2 above will be due to the sampling process from ERA5 to AIRS L2Sup levels to the final output ERA5-FCST grid.

Step 1 includes some contributions from horizontal resolution since the ERA5 IFS does not use a 0.25° latitude-longitude grid, but the horizontal resolution is similar. The comparison will use the grid cells in the red box from Figure S1, which displays the ERA5 product CAPE at overpass time. The selected area provides a broad range of CAPE during the 2019-07-19 case study.

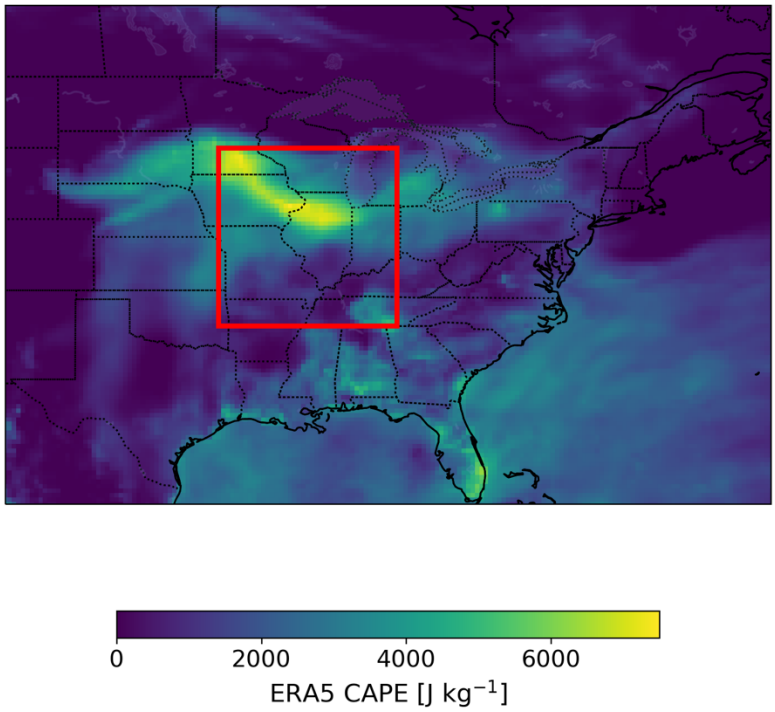

Figure S1. 2019-07-19 ERA5 product CAPE at AIRS overpass time. The CAPE results below use the region inside of the red box.

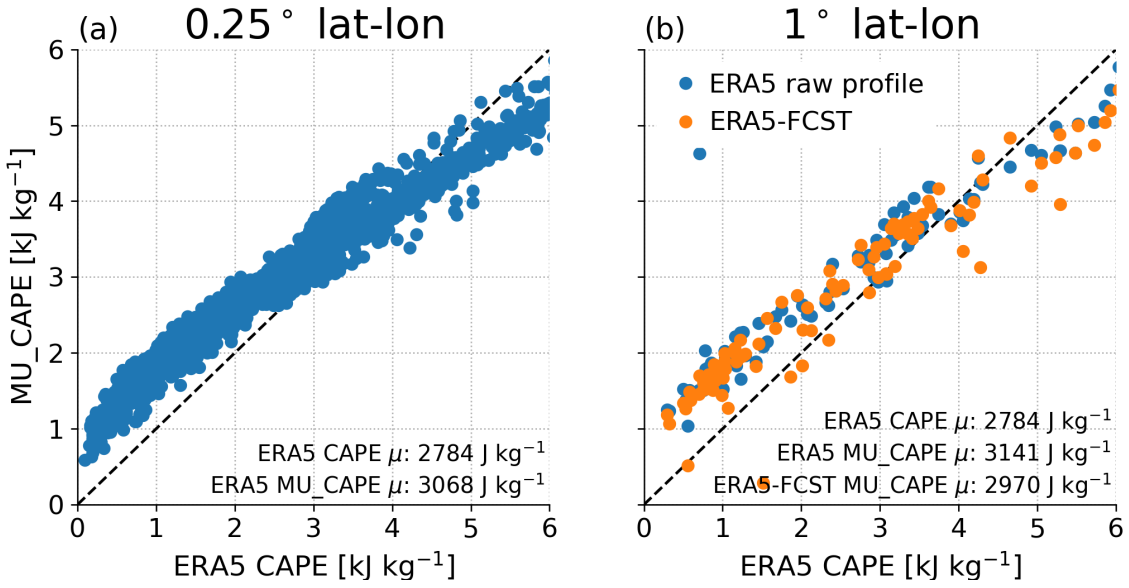

Figure S2. SHARPpy-calculated MU_CAPE as a function of ERA5 product CAPE. (a) At 0.25° resolution, with SHARPpy using the publicly downloadable ERA5 3-D profiles, (b) at 1° resolution. For the 1° resolution, the blue points are values calculated from the profiles at the ERA5 3-D vertical resolution but after averaging to 1° in the horizontal. The orange points are those calculated from the ERA5-FCST gridding at overpass time, which is labelled as ERA5-overpass in the main manuscript. Text in the bottom right corner of each panel reports the region-mean CAPE for each calculation method.

Inter-product CAPE comparisons are shown in Figure S2. Panel (a) shows that compared with ERA5 values, the combination of SHARPpy and coarser vertical resolution results in MU_CAPE that is relatively higher in low-CAPE environments, but relatively lower in high-CAPE environments. Overall, the SHARPpy mean CAPE is higher, but only by <10 %. In panel (b), the same pattern can be seen both when MU_CAPE is calculated at 1° resolution on the ERA5 vertical grid or from the ERA5-FCST grid. The ERA5-FCST calculation introduces more scatter than when using the ERA5 profile.

Importantly, the main paper analysis Figs. 10—13 did not use absolute values of convective parameters, but rather binned grid cells by their percentile of CAPE or CIN. The results depend only on the relative ranking of grid cells, so biases or nonlinearities in the relationship between CAPE calculated in different ways will not affect the conclusions, provided that the relationship is monotonic. We now estimate how differences in resolution and CAPE calculation method affect the main conclusions by considering how consistently grid cells are assigned to each bin. The process is schematically shown in Figure S3, where the ERA5 product CAPE and SHARPpy-calculated MU_CAPE are binned. The figure bins each product into quartiles because differences are easier to view, the main paper results use a range of bin sizes.

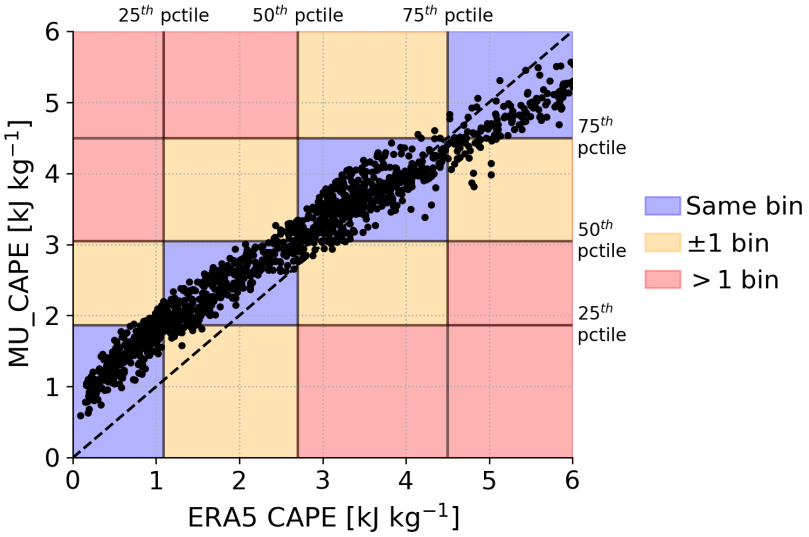

Figure S3. Data from Figure S2 (a) with areas shaded to illustrate the consequences for grid-cell assignment to CAPE bins as in the main manuscript. For ease of illustration, the data are split into quartiles here, but the main manuscript uses different percentiles. Points are grid cell values and those that fall in blue areas are where both the ERA5 product and SHARPpy CAPE values agree on the bin. Those that fall within orange areas disagree by ±1 bin. If any fell within the red areas, they would disagree by ±2 bins or more.

Any points within the blue shaded areas are assigned to the same bin, regardless of whether the ERA5 product or SHARPpy-derived values are used. Those that fall within the orange are within ±1 bin, and those within the red areas would disagree by two or more bins. The rate of disagreement depends on the size of the bins (finer binning increases the disagreement rate) and on the scatter between estimates (larger scatter increases disagreement rate). The number of valid over-land grid cells that fall within each bin for the main-paper percentile ranges is reported in Table S1.

Table S1. Counts of how many footprints fall within each combination of ERA5 product CAPE and ERA5-overpass MU_CAPE bin, with the latter calculated using SHARPpy. For example, the top left entry represents how many grid cells fall between the 0—70th percentile in both ERA5 and ERA5-overpass. Cells are shaded to match the colouring in Figure S3: blue represents agreement, orange represents disagreement by ±1 bin, and red represents disagreement by >1 bin.

	ERA5-overpass + SHARPpy MU_CAPE					
ERA5 CAPE	>0	>70	>80	>90	>95	>99.5
>0	49016	1935	459	73	38	2
>70	2444	3632	1080	130	74	1
>80	63	1782	4613	756	140	6
>90	0	12	1140	2001	525	2
>95	0	0	68	719	2400	125
>99.5	0	0	0	1	135	233

The table shows that most footprints would be assigned to the same bin using either the ERA5 product CAPE, or the MU_CAPE derived from ERA5 3-D fields. Over the whole table, 84.1 % of grid cells are assigned to the same bin by both CAPE calculation methods, and 98.5 % of grid cells are assigned to within ±1 bin.

In summary, there is good agreement in the ranking of CAPE between that reported in the ERA5 product and that calculated at the ERA5-FCST spatial resolution and using SHARPpy. We therefore anticipate only small differences are introduced by the changes in horizontal and vertical gridding across the products considered in this study. The most convincing result is that MU_CAPE and MU_CIN calculated on the ERA5-FCST spatial grid are genuinely predictive of ERA5 precipitation, suggesting that their resolution is appropriate for studying convection.

Results may differ for an AIRS-FCST product because of differences in its effective vertical resolution (which differs from the product L2Sup layering) and because of retrieval uncertainties. These issues are beyond the scope of the present paper, which specifically targets the trajectory-enhancement component of FCST products. Preliminary work generated a partial AIRS-overpass product from v7 L2Sup data at the same 1° lat-lon and 30 hPa vertical gridding as ERA5-FCST. Approximately 80 % of the footprints from Table S1 have been processed, for which agreement between AIRS-overpass MU_CAPE and ERA5 product CAPE is 72.6 %. Once disagreements within ±1 bin are included, the agreement rises to 90.3 %. A more detailed analysis will be performed as part of the full AIRS-FCST development.

2 AIRS vertical resolution

The effective vertical resolution of sounding instruments such as AIRS is limited by the amount of information contained in the measured spectra. A common method to report an "effective" vertical resolution is based on the averaging kernel **A**, which is discussed in the Irion et al. (2018) citation provided in the main paper. The matrix **A** changes with every measurement and the effective vertical resolution depends on the atmospheric structure. Here we assume a typical effective vertical resolution following Irion et al. (2018)'s statement regarding *T* and *q* profiles: "*From this fitting approach, shown in the third panel of Fig. 5, the vertical resolution is about 1 to 1.5 km from the ground to about 300 mb*".

We estimate the effect of vertical resolution of that order of magnitude by reprocessing the July 2019 ERA5-Overpass profiles. The profiles are smoothed vertically with a boxcar filter of pressure thickness ΔP of either 90 hPa or 150 hPa. The smoothed profiles are remapped onto the ERA5-FCST grid of ΔP =30 hPa then MU_CAPE is recalculated and compared with the main-manuscript values. The smoothing reduces the effective resolution of the profiles to values similar to the 1—1.5 km reported in Irion et al., even if the outputs have been interpolated onto a finer resolution. This is analogous to the use of the many AIRS L2 support levels in ERA5-FCST and AIRS-FCST.

An important caveat is that the **A** matrices reported with AIRS products refer to the information gained in updating the retrieval prior. Since the AIRS version 7 retrieval prior is built from AIRS measurements, the prior represents some additional information from the instrument, so the true effective vertical resolution of AIRS retrievals should be finer than

that obtained from **A**. Our selected ΔP of 90—150 hPa, which is similar to the 1—1.5 km reported in Irion et al., is therefore coarser than the likely true vertical resolution of the version 7 AIRS retrievals.

We report statistics for the July data only for ΔP smoothing of 90 hPa in Table S2 and for 150 hPa in Table S3. As expected, performance degrades with resolution. For 90 hPa smoothing, there is exact agreement 72.1 % of the time, and agreement within ±1 bins 93.0 % of the time. For 150 hPa smoothing, the agreements fall to 64.2 % (exact) and 82.4 % (±1 bin). Real-world retrievals will have coarsened effective vertical resolution and may therefore fail to identify certain thermodynamically important features. Nevertheless, even after extreme smoothing, they still correctly classify a large portion of profiles as either "high" or "low" CAPE conditions, which is the requirement for our classifier approach.

Given the additional information contained in the prior, we expect that the 90 hPa smoothing is more likely to be representative of reality overall. It should also be noted that the effective resolution reported here is instrument dependent, and may change with instrument spectral sampling or noise. Separate tests would need to be performed for candidate instruments to understand whether a trajectory enhanced FCST product developed from their data is likely to be useful.

Table S2. Counts of how many July 2019 profiles fall within each MU_CAPE percentile bin using the main-manuscript ERA5-Overpass approach versus after smoothing the ERA5 profiles in pressure coordinates with a 90 hPa moving boxcar filter. Cells are shaded to match the colouring in Figure S3: blue represents agreement, orange represents disagreement by ±1 bin, and red represents disagreement by >1 bin.

	ERA5-Overpass MU_CAPE after 90 hPa smoothing					
ERA5-Overpass	>0	>70	>80	>90	>95	>99.5
>0	5986	502	155	0	0	0
>70	366	201	343	39	0	0
>80	214	165	270	269	31	0
>90	60	54	117	103	141	0
>95	17	27	63	64	245	11
>99.5	0	0	1	0	10	37

Table S3. Counts of how many July 2019 profiles fall within each MU_CAPE percentile bin using the main-manuscript ERA5-Overpass approach versus after smoothing the ERA5 profiles in pressure coordinates with a 150 hPa moving boxcar filter. Cells are shaded to match the colouring in Figure S3: blue represents agreement, orange represents disagreement by ±1 bin, and red represents disagreement by >1 bin

	ERA5-Overpass MU_CAPE after 150 hPa smoothing					
ERA5-Overpass	>0	>70	>80	>90	>95	>99.5
>0	5522	526	468	119	8	0
>70	494	154	150	105	46	0
>80	396	156	164	124	109	0
>90	152	70	95	67	90	1
>95	77	43	70	59	159	19
>99.5	2	0	2	1	15	28

Table S4. Total precipitation (*tp*) statistics for ERA5-FCST grid cells where CAPE>99.5th percentile and CIN<70th percentile. Each row represents the values calculated from a different combination of parcel and whether the absolute or enhanced parameters were used. MU = most unstable, MML = mean mixed layer, entries beginning with "d" (e.g. dMU) represent the enhanced values where each grid cell has had the daily mean subtracted. Left-most data column is the mean precipitation in that CAPE-CIN bin, and the next 3 columns are the frequencies calculated for precipitation rate thresholds of 3, 4 and 5 mm hr^{-1}. The bottom row are those same statistics calculated for all grid cells with valid CAPE and CIN in all ERA5-FCST timesteps.

		Frequency [%]		
Parcel	Mean *tp* [mm hr^{-1}]	*tp* > 3 mm hr^{-1}	*tp* > 4 mm hr^{-1}	*tp* > 5 mm hr^{-1}
dMU	1.00	10.44	6.4	3.55
MU	0.92	9.11	5.67	3.04
dMML	1.00	9.92	6.66	3.97
MML	1.04	10.41	6.46	3.95
Full sample	0.09	0.29	0.12	0.05

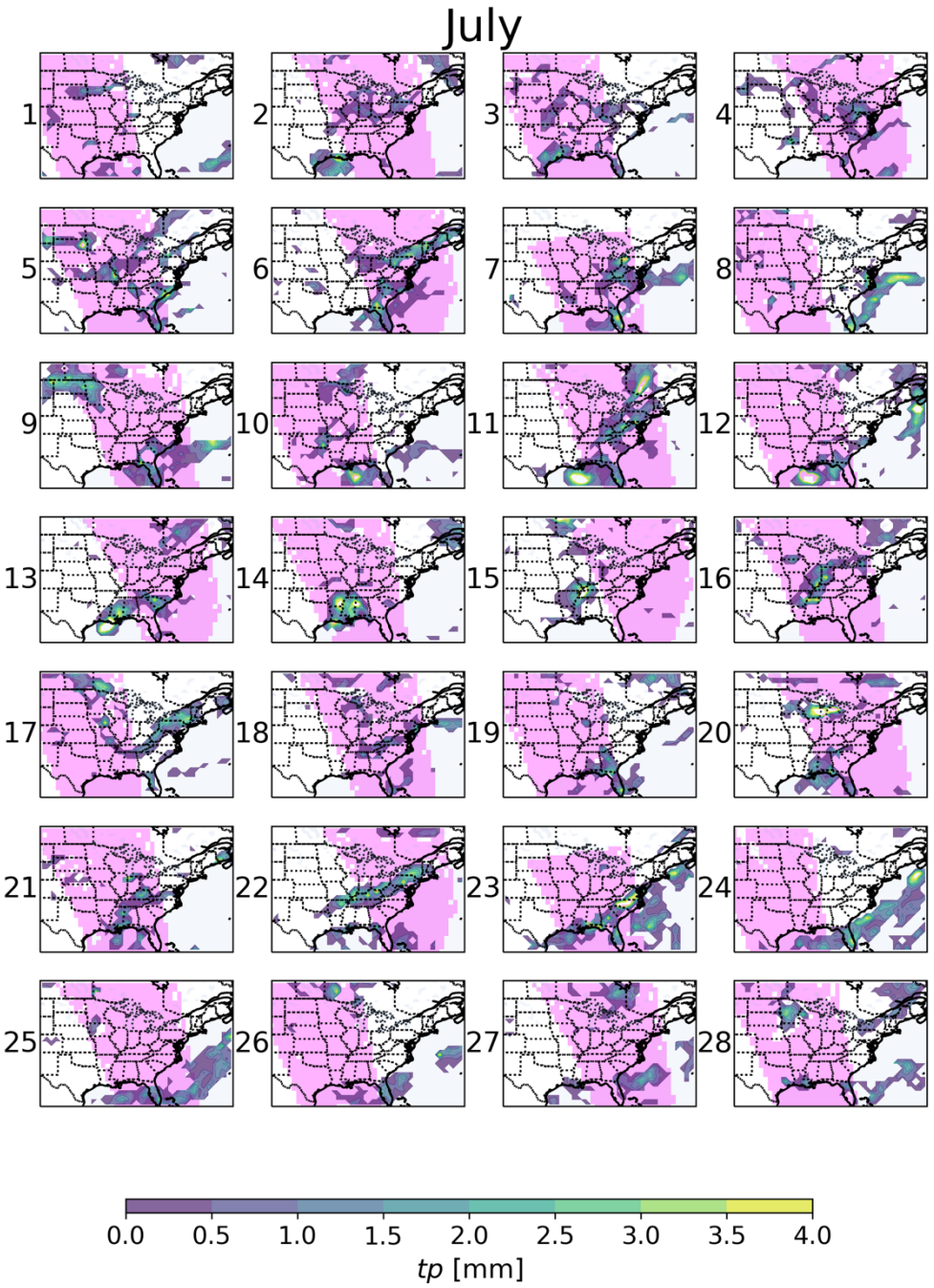

Figure S4. ERA5 hourly precipitation rate for 1—28th July 2019 at the mean AIRS footprint time on each day. The pink shading denotes where there are sufficient valid AIRS retrievals for the ERA5--FCST product to report a valid CAPE.

140

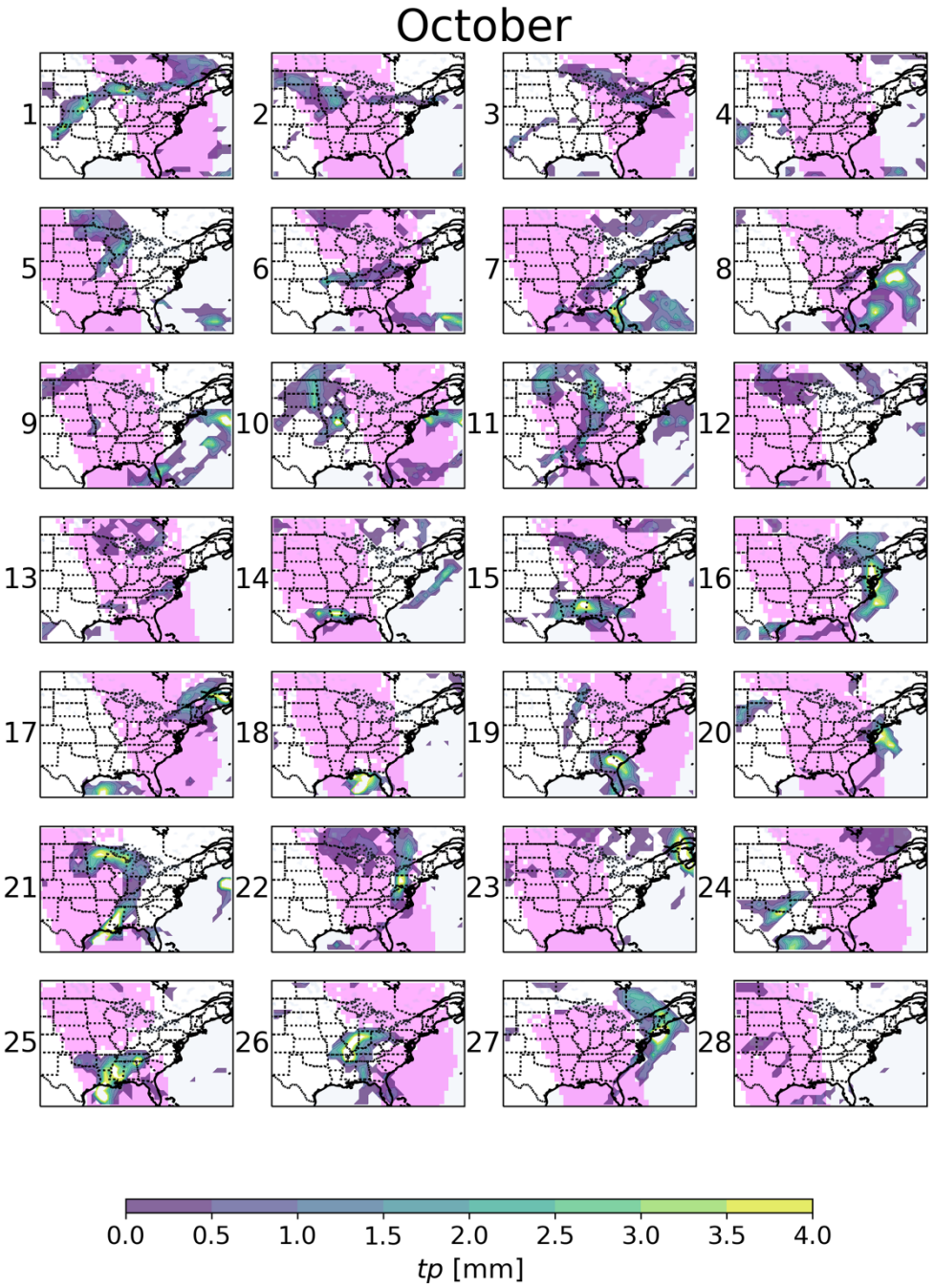

Figure S5. ERA5 hourly precipitation rate for 1—28th October 2019 at the mean AIRS footprint time on each day. The pink shading denotes where there are sufficient valid AIRS retrievals for the ERA5--FCST product to report a valid CAPE.

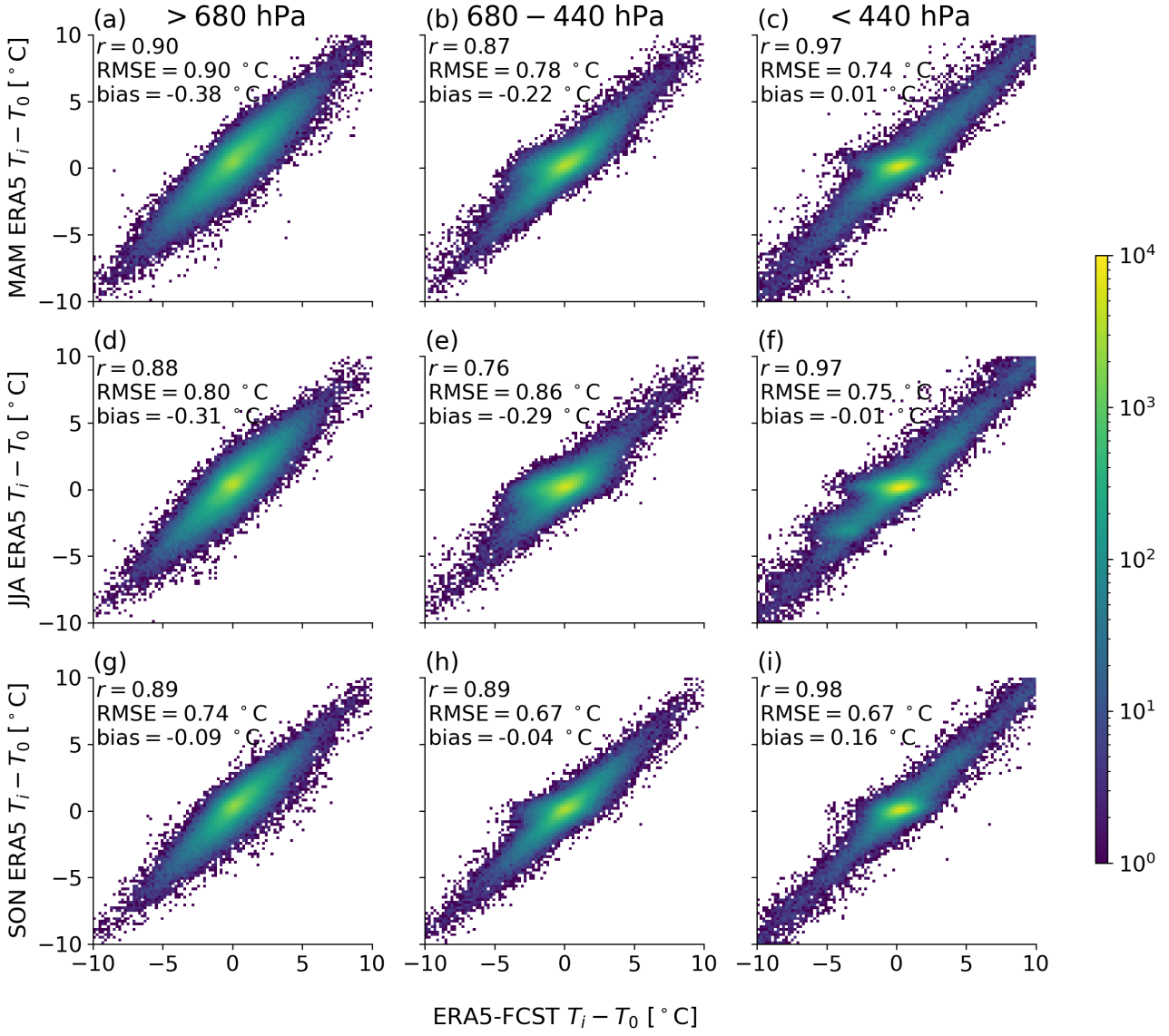

145

Figure S6. 2d histograms of change in layer-mean *T* relative to overpass time, ERA5 on *y* axis and ERA5-FCST on *x* axis. Columns are each season: (a—c) MAM, (d—f) JJA, (g—i) SON. It is expected that sub-grid convection in ERA5 causes mid- and potentially upper-layer heating relative to ERA5-FCST and that this process explains the bulges near *y*=0 where *x*<0. Convection is most common in JJA, and its mid-layer panel (e) shows larger RMSE and smaller *r* than either (b) or (h), consistent with the *y*=0
150 **feature being convection-driven.**

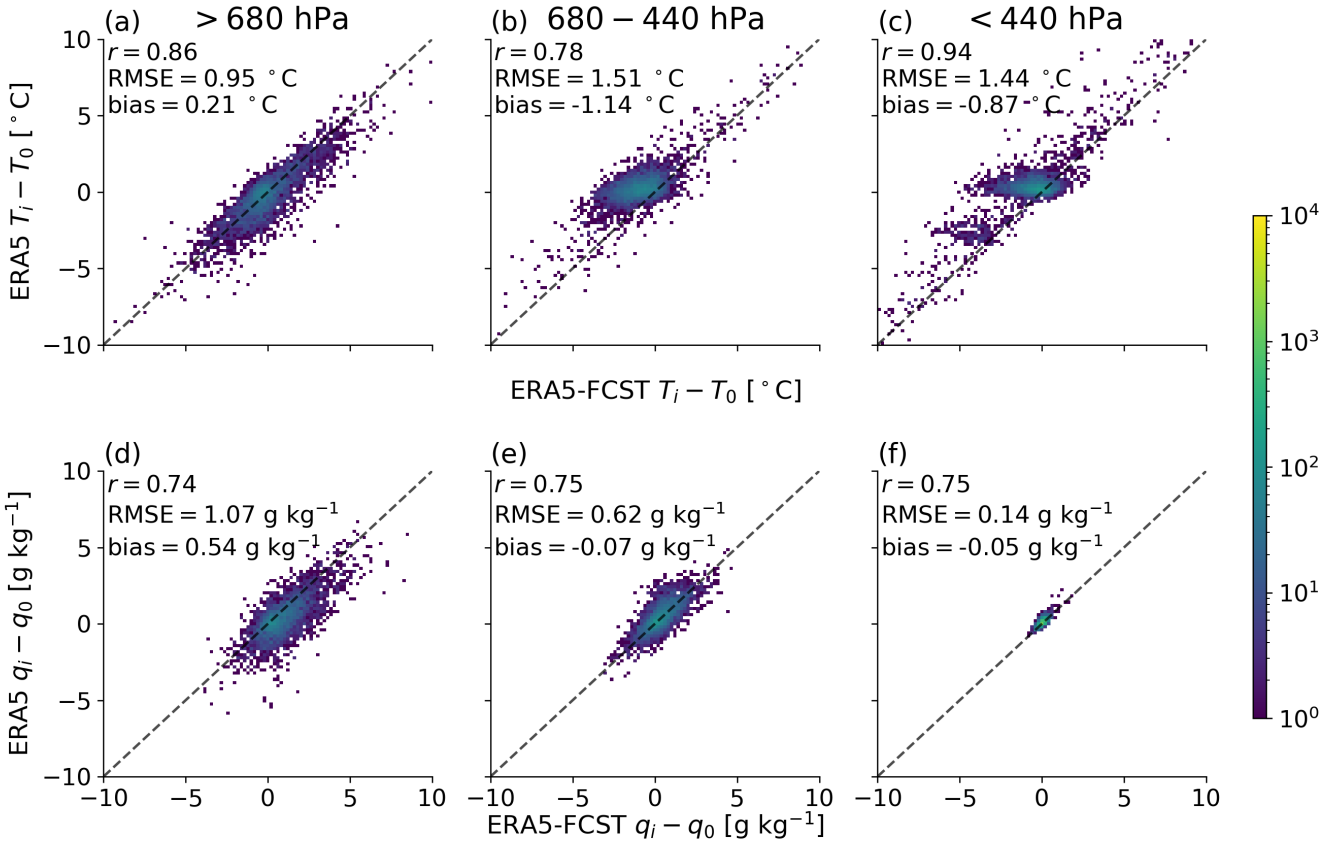

Figure S7. As Figure S6 but only during hours in which precipitation exceeds the 99th percentile of the sample, or 1.8 mm hr^{-1}. The main-text hypothesis proposes that some of these precipitation events will be convective, and involve efficient vertical heat transport. In which case, temperatures in the mid- and upper levels in ERA5-FCST should be cooler than in ERA5, since the sub-grid vertical heat transport is neglected in ERA5-FCST. The results show that this is the case: (b) ERA5-FCST is -1.14 °C cooler than ERA5 from 680—440 hPa , compared with -0.19 °C for the full sample including non-raining cases. (c) ERA5-FCST is -0.87 °C cooler where *P*<480 hPa during these wet timesteps, compared with +0.03 °C warmer during all timesteps in the main paper.

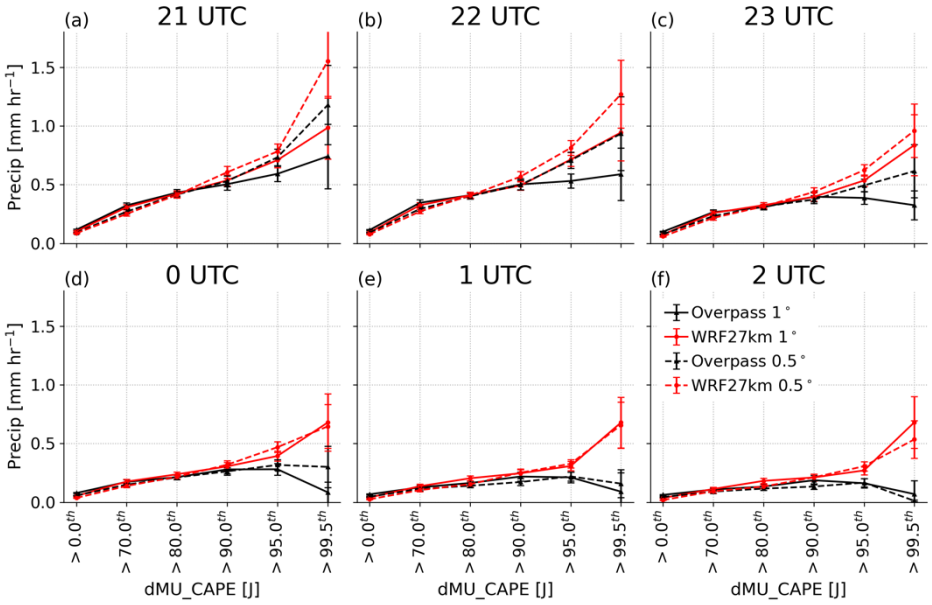

Figure S8. JJA data, mean precip in grid cells binned by percentile of dMU_CAPE. Values are for a FCST product at horizontal resolution of 1° (solid) or 0.5° (dashed). Spatial averaging smooths the *tp* distribution, so more extreme *tp* values are expected at 0.5° than 1° resolution, which may explains the higher dashed lines relative to the solid lines during 21—23 UTC.

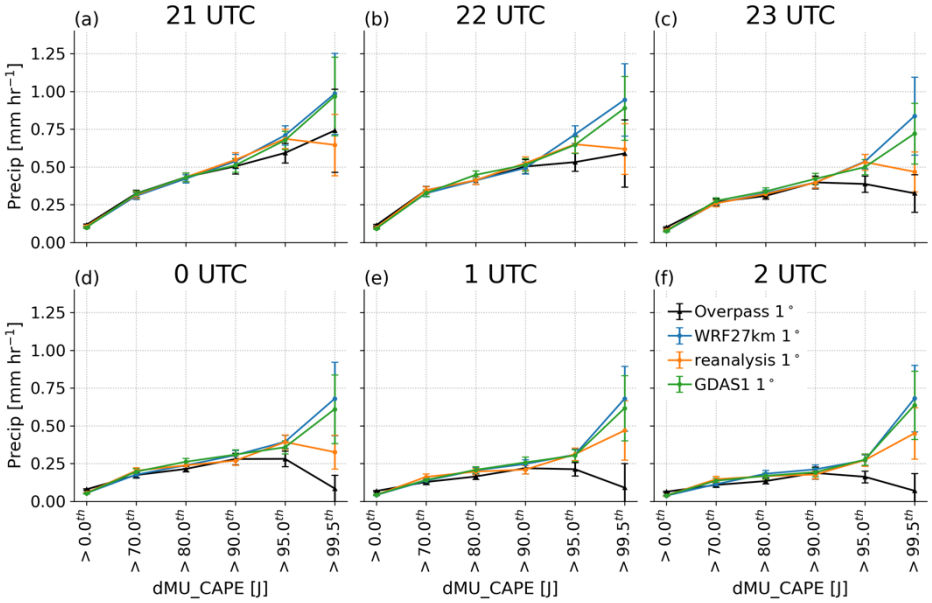

Figure S9. As Figure S8 but for different NWP wind sources. Black line represents overpass time values. The coloured lines are from FCST products generated with WRF27km, reanalysis and GDAS1 NWP winds, using the products stored by ARL for HYSPLIT. Grid cells are included where all product timesteps return a valid MU_CAPE, and differences in NWP winds may therefore cause some differences in sampling between each line.